

Comparing the efficiency of different structural skeletons for base-isolated domes

Sara CASCIATI *

SIART srl, Pavia, Italy

Abstract. The structural concept of the dome dates back to the Pantheon in Rome. It is used as the cover of many churches and mosques all around the world. Light solutions, with a well-visible dome-shaped truss skeleton, are often preferred in modern architecture. Base isolation techniques can be adopted to mitigate the seismic effects. This paper aims to investigate the efficiency of different designs for the truss skeleton. To solve the problem, one has to assign the constraints, the materials and the geometry of the dome, its supporting structure and the isolation devices (number, locations, and type). The screening of the effects of different scheme assumptions on structural behaviour provides a better insight into the problem.

Key words: base isolation; design requirements; dome; isolation device; passive structural control.

1. INTRODUCTION

The structural concept of the dome dates back to the Pantheon in Rome, the Agia Sophia monument in Istanbul, the Holy Peter Church in the Vatican, the Taj Mahal in Agra and the cover of many churches and mosques all around the world. Recently some of them were base-isolated to mitigate the local seismic risk (see [1], among others).

The same term “dome” also applies to the current architectural solution to provide “bubbles” for both meetings of a few persons or general assemblies of communities. These bubbles come with a continuous shell, often made from transparent material, supported by a well-visible truss skeleton. Again, base isolation can be adopted to mitigate seismic risk mitigation [2].

It is worth noticing that domes of this type are often adopted to provide complementary spaces to educational facilities, with the consequent need for an accurate risk assessment [3–5] of their performances.

The market offer frequently refers the designer to a geodesic scheme for the tubular skeleton. A geodesic dome is a hemispherical thin-shell structure (lattice-shell) based on a geodesic polyhedron. This makes them different from each other. There is extensive literature on geodesic schemes, and it is impossible to compile an exhaustive list of references. Attention is generally paid to their topology and geometry [6–9], to their structural optimization [10–13] or their structural behavior [14]. The response to the seismic excitation was studied in [15, 16].

This paper aims to compare the response of such geodesic dome, when base-isolated, with those of different mechanical models, in terms of node displacements and stress distributions in the truss. Nevertheless, a comparison of different structural

schemes is only possible if some modifications of the anchorage in the geodesic design facilitate the introduction of the base isolation system. First, the stress distribution across the structural members is investigated due to the gravity action and other operational loads. Different ground motion signals are then applied to the structure and, again, the structural response is estimated. The analyses are carried out in the presence of the isolation devices and their effectiveness is compared with reference to the considered truss options. In all the studied cases, the devices are idealized as orthotropic elastic volumes [2].

2. BUILDING THE APPLICATION

2.1. Base isolation

Base isolation is not the direct focus of this paper. Therefore, for the sake of reducing any model complication, a scheme allowing a linear treatment of the dynamics of a base-isolated system is pursued. For this purpose, the selected devices are elastomeric bearings, i.e., multi-layered, high-damping, rubber disks laminated with reinforcing thin steel plates. Indeed, a homogeneous orthotropic elastic material adequately models such a device. One needs the thickness of the isolator, the global stiffness along two directions in the horizontal plane and the stiffness along the vertical direction.

Since the pioneering books by Kelly [17, 18], several scientific [19] and technical [20, 21] papers were published on this matter [2]. Nevertheless, for the extraction of the three required quantities, the procedure in [22], strictly coupled with UBC97 [23] and the guidelines of Section 8 in reference [18], are conveniently adopted.

The known design variables are:

- the bearing load W ;
- the properties of the high-damping compound, namely G , the shear modulus of the elastomer, and the associated effective damping β_{eff} ;

*e-mail: sara@dipmec.it

Manuscript submitted 2022-05-23, revised 2022-09-20, initially accepted for publication 2022-09-25, published in June 2023.

- T_D = effective period, in seconds, of the seismic-isolated structure at the design displacement in the direction under consideration, as prescribed by

$$T_D = 2\pi \sqrt{\frac{W}{gk_{\min}}} \quad (1)$$

with g denoting the gravity constant, 9.81 m/sec^2 and k_{\min} the minimum horizontal stiffness of the device;

- D_{TM} = total maximum displacement.

The total thickness d of the rubber is linked with D_{TM} by

$$d = \frac{D_{TM}}{\gamma} \quad (2)$$

with the maximum shear strain, γ , usually taken as 150%.

One assumes a value for T_D and D_{TM} ; then equation (1) provides k_{\min} and d . Finally, the third equation provides the full cross-sectional area A :

$$k_{\min} = \frac{GA}{d}. \quad (3)$$

The vertical stiffness is conveniently selected in several orders of magnitude larger than the horizontal stiffness.

2.2. Schemes for the dome 3D-truss assemblage

An Italian producer writes on its webpage: the company “realizes geodesic domes with steel tubulars, which can have a diameter between $26 \times 1.5 \text{ mm}$ and $60 \times 3 \text{ mm}$, and a tarpaulin in white, transparent, opaque, or customizable PVC, also by combining them . . . The geodesic domes cover an area that can vary from 45 square meters to 3220 square meters in total, with a maximum height of 20 m; stability and resistance are guaranteed even in case of snow (snow load up to 75 kg per m^2) and strong wind (up to 120 km/h)”.

Four remarks apply:

1. A solution with the shield in glass is also provided.
2. The radius spans between 3.79 m to 31.92 m.
3. There is no mention of the seismic response.
4. Only geodesic domes are proposed.

That specific kind of geodesic dome is sketched in the photo of Fig. 1. One sees equilateral triangles whose sides are arcs of circumferences all from maximum circles, i.e., with the center in the center of the sphere and the radius of the sphere.

The way the geometry is generated uses the drawing of the necessary maximum circles toward a sequence of triangles within a larger boundary hemisphere sector. Figure 2 is a sketch of a finite element model for it. It is not complete since it will not be analyzed, having been introduced just for sake of clarification. In the l.h.s, the hemisphere is seen from the top. The circumference at the base is divided into six equal arcs. Three of them in sequence form a semi-circumference, which is rotated at 30° , 60° , 90° , 120° and 150° around the diameter connecting the ends.

Attention is then focused on the single $1/6$ sector: the first triangle on the top is not actually a triangle, but the surface of the hemisphere sector is limited by arcs from three maximum circles. It has as its basis an arc from the maximum semi-circle obtained by the rotation of 60° and the lateral sides are

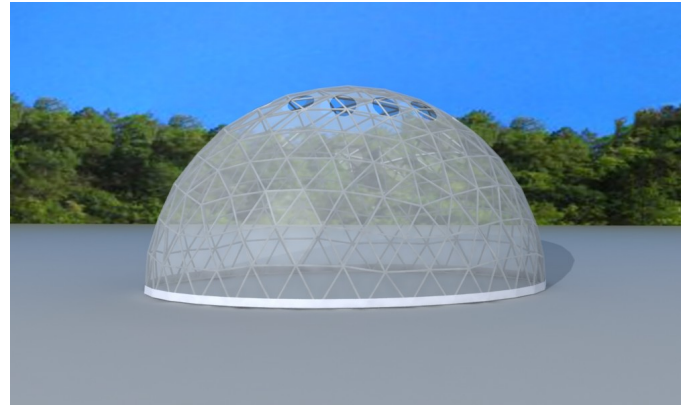


Fig. 1. Example of the transparent geodesic dome (re-elaborated from the internet)

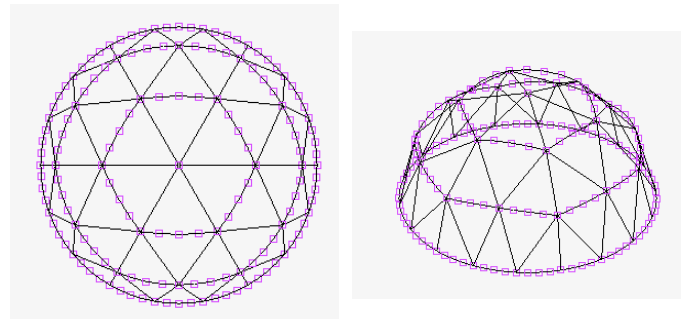


Fig. 2. Sketch of the finite element model of a geodesic dome

arcs from the maximum semicircles limiting the sector (i.e., the meridians obtained by rotations of 90°). As said, this detail is not refined in the r.h.s. of Fig. 2: just the secants serve as lateral elements. The refinement would require the introduction of nodes on the circles, not just a subdivision of the secant elements.

Below this top triangle, one finds a sequence of three triangles, two with the vertices upward and one with the vertex downward. The basis of the latter one is on the maximum circle obtained by rotation of 60° , while the former ones are on the maximum circles obtained by rotation of 30° . The lateral sides are always arcs from maximum circles, not explicitly drawn.

Finally, below the set of three triangles, there are five triangles, three with the vertices upward and two with the vertices downward.

Assume that the initial rotation of semicircles is no longer 30° by 30° but 15° by 15° . Each sector would include the following series of triangles: 1, 3, 5, 7, 9 and 11.

In view of the developments reported within this paper, the model of Fig. 2 offers the main inconvenience that the symmetry with respect to two orthotropic axes is lost. Moreover, since the sequence of triangles 1, 3 and 5 involves 24 nodes at the bottom level, one should adopt 24 base isolators that are an excessive number. The alternative would be six base isolators, a solution not offering the same symmetry advantages as eight base isolators. This is why the model of the geodesic dome adopted in this paper does not see the construction over a $1/6$

Comparing the efficiency of different structural skeletons for base-isolated domes

sector but over a 1/8 sector. The consequence is that the triangles are no longer appearing as equilateral. A rotation policy of 22.5° by 22.5° is adopted, with the triangle sequence being 1, 3, 5 and 7 (Fig. 3).

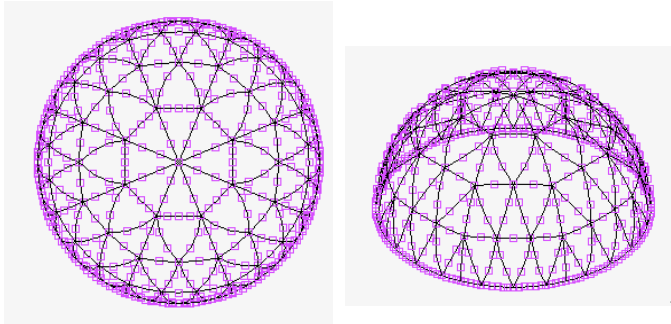


Fig. 3. Finite element model of a geodesic dome built over a sector of 45°

Inspection of Fig. 3 leads us to two main remarks:

- (a) Given the purpose of identifying eight supporting points, the sequence of triangles between the basis and the first parallel from the bottom has no structural motivation; the external shield will result as appended to the first parallel.
- (b) The eight supporting points are identifiable as the bottom vertices of the triangles in the middle of each sector.

These two remarks produce the first structural model, as given in Fig. 4, while a variant comes as follows. After the removal of the eight elements ending in the node at the top of the dome, a ring of elements is introduced between the starting nodes to model the standard hole at the top of a classical dome.

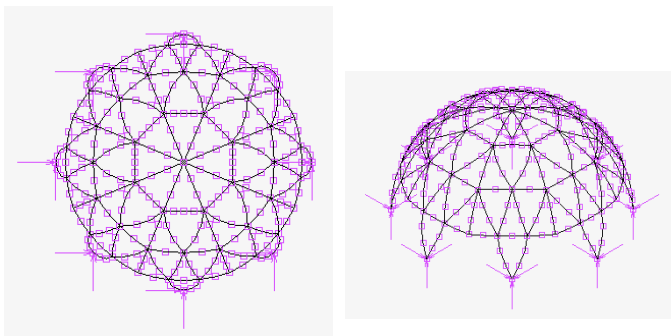


Fig. 4. Finite element model of a geodesic dome built over a sector of 45°, after removal of the bottom layer

The material is standard steel, while the geometric section is tubular, with diameter and thickness from the market offer.

The main structural properties are summarized in the first two rows of Tables 1 and 2. The upper row considers the model in Fig. 4, while the other row covers the variant.

The performance of the dome in Fig. 4 will be compared with three further models. Figure 5 provides the construction rationale and Fig. 6 further models. Also for them, the structural properties are in Tables 1 and 2, but the variant was only considered for the model of Fig. 6a.

Table 1

Summary of the static analyses for the domes before base isolation. For each model, the diameter and the thickness of the tubular elements are provided in cm. The first two models come with two rows, the second one being associated with the variant with the hole on the top

Model	Base vertical reaction (dead load) [kN]	Vertical displacement on the top (dead load) [cm]	Horizontal displacement on the top (0.1 dead load) [cm]
Geodesic 4.83 × 0.32	2.195 2.183	0.3391 0.3260	0.9817 0.9803
Model (a) 3.37 × 0.26	1.762 1.756	0.2957 0.2888	0.3252 0.3262
Model (b) 4.83 × 0.32	2.235	1.0908	4.0776
Model (c) 4.83 × 0.32 6.03 × 0.32	1.767 2.206	1.7845 1.1538	3.6853 2.3689

Table 2

Modal frequencies from the analyses for the domes before base isolation. For each model, the diameter and the thickness of the tubular elements are provided in cm. The first two models come with two rows, the second one being associated with the variant with the hole on the top

Model	First couple of flexional modes [Hz]	Second couple of flexional modes [Hz]	Torsional mode [Hz]
Geodesic 4.83 × 0.32	1.557 1.562	5.898 4.391	2.648 (3) 2.647 (3)
Model (a) 3.37 × 0.26	2.534 2.538	5.494 3.730	3.573 (3) 3.573 (3)
Model (b) 4.83 × 0.32	0.7538	3.362	1.201 (3)
Model (c) 4.83 × 0.32 6.03 × 0.32	0.789 0.985	3.17 3.954	1.278 (3) 1.595 (3)

Model (a) is conceived to preserve one of the two main characteristics of a geodesic dome: to result from the assemblage of arcs from principal circles. Each of the semicircles connecting two opposite supports is rotated seven times at 22.5°. The model violates the second requisite, for being a geodesic dome: the mesh must be composed of triangles only. Also in this case the variant was considered. As one can see in Tables 1 and 2, the responses of the variants are not significantly different from each other and the hole on the top is neglected in the remaining part of this paper.

Model (b) is conceived by introducing meridians and parallels. In model (c) the former is removed. The model in Fig. 6c

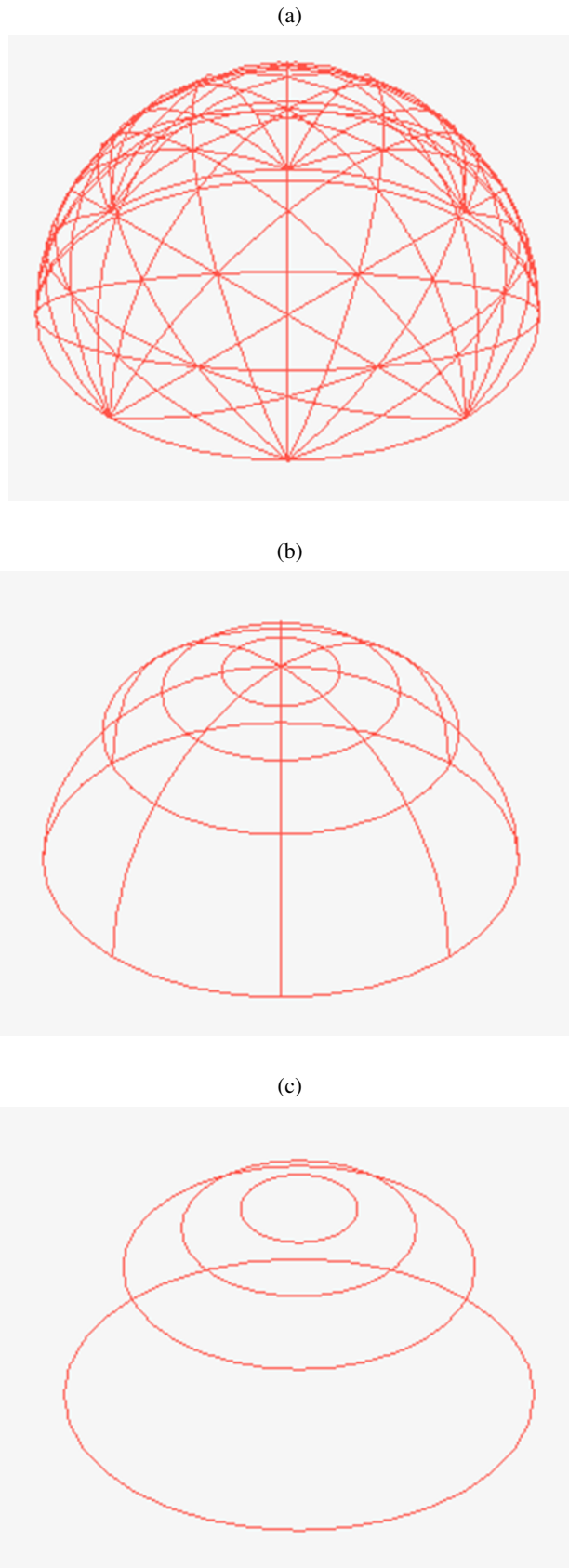


Fig. 5. Graphical support to the geometrical construction of the dome models: (a) modified geodesic system; (b) system with supporting parallels and meridians; (c) system with supporting parallels but no meridians

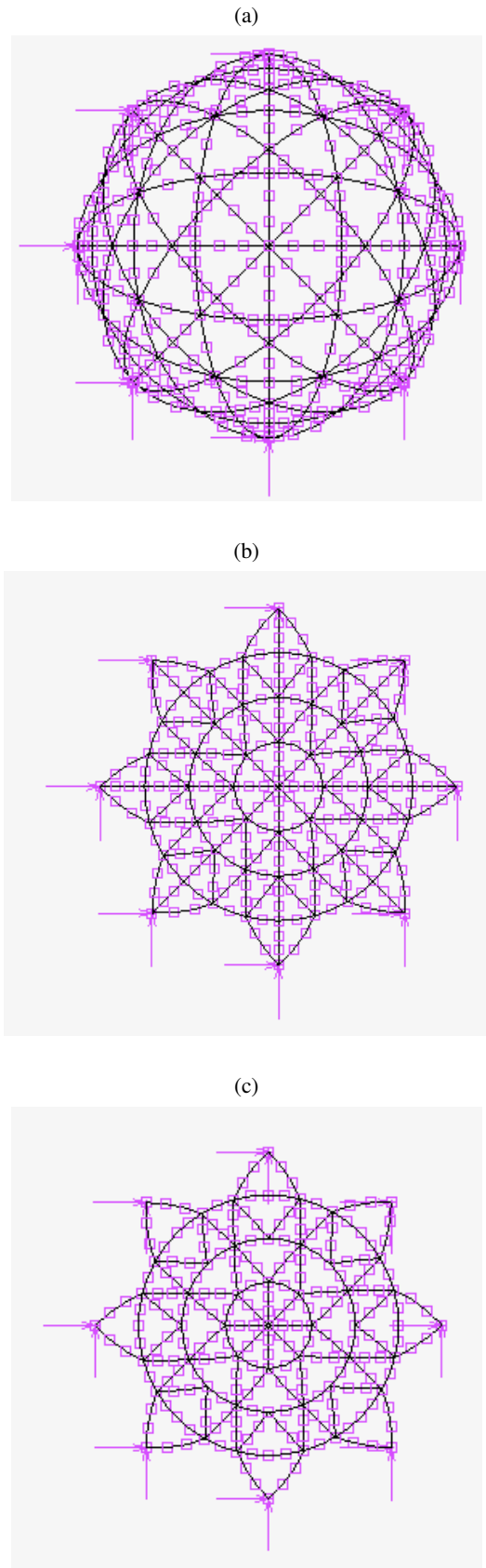


Fig. 6. Top-down view of the finite element models: (a) modified geodesic system; (b) system with supporting parallels and meridians; (c) system with supporting parallels but no meridians

Comparing the efficiency of different structural skeletons for base-isolated domes

was designed by using two sizes of the geometrical section, but only the heavier is retained, thus preserving a similar weight for all the considered models. Model (a) is lighter than the others since the architecture results in a stiffer scheme.

3. DESIGN OF THE DEVICE

With reference to the geometry reported in the last section, one can now proceed to the design of the base isolation device. The bearing load W is eight times the values in the first column of Table 1, i.e., something less than 18 kN.

Assume the effective period $T_D = 2.5$ sec, equation (1) provides

$$k_{\min} = (2 \times 3.14/2.5)^2 W/g = 11.358 \text{ kN/m},$$

i.e., 1.420 kN/m per device.

It is worth noting that considering the snow load (1 kN/m^2), the bearing load would result in $18 + 3.14 \times 10 \times 10 \times 1 = 332 \text{ kN}$, to be considered when designing the vertical stiffness. The former value is consistent with the absence of snow in conjunction with the soliciting horizontal action.

The total maximum displacement D_{TM} is 0.3 m. From equation (2) one has $d = 0.2$ m, for $\gamma = 1.5$. From equation (3) and $G = 0.4 \text{ MPa}$ one has $A = 0.2 \times 0.00142/0.4 = 0.00071 \text{ m}^2$, i.e., a radius of 0.0106 m, which is inconsistent with the value chosen for D_{TM} .

Each device has a cylindrical shape with a radius of 0.3 m. The elastic properties of the orthotropic modelling material are set to provide 1.456 kN/m as horizontal stiffness and 3239 kN/m as vertical stiffness. Note that in the market offer, the ratio between the latter and the former values is usually in the range of 1000–2500.

4. NUMERICAL SIMULATIONS

Each dome model was associated with a set of eight devices as was introduced in the previous section. The structural skeleton of the dome is modelled as a standard steel. The isolation devices are cylinders of orthotropic material (with higher stiffness along the vertical axis) with elastic parameters calibrated to obtain the device global stiffness given in Section 3. A cable joins each anchorage point with the two neighboring ones. The resulting models underwent first a static analysis and then a dynamic modal analysis with the results summarized in Tables 3 and 4.

Then, dynamic transient analyses were carried out with time step 0.01 s. The damping was only introduced for the device and set to 15%. The excitation was synchronous on the eight devices and was a piece-wise linear sequence of three cycles of intensity 1, three of intensity 2 and three of intensity 3, followed by half signal at rest. The period of the cycles was assigned as 0.125, 0.25, 0.5 and 1 second (corresponding to the frequencies 8, 4, 2 and 1 Hz, respectively) for four different analyses. The resulting displacement time histories for the geodesic dome are summarized in Fig. 7. Table 4 also summarizes the oscillation of the worst axial force for the different models and the different excitations.

Table 3

Updated frequencies in [Hz] for the structural systems enclosing the isolation devices

Model	First flexional couple	Torsional mode	First dome couple	Second dome couple	Third dome couple
Geodesic	0.3165	0.3.77	1.741	1.931	2.672
1	0.3402	0.3892	2.243	2.407	4.017
2	0.3088	0.3891	1.324	1.532	1.696
3	0.3135	0.3962	1.605	1.933	1.954

Table 4

Worst axial force in [kN] at the bottom elements under the gravity load and its oscillation during the ground excitations for different frequencies

Model	Gravity load	1 [Hz]	2 [Hz]	4 [Hz]	8 [Hz]
Geodesic Node 831	-1.14	-0.177 / 0.191	-0.599 / 0.539	-0.382 / 0.447	-0.716 / 1.058
1 Node 1151	-0.458	-0.104 / 0.114	-0.153 / 0.232	-0.874 / 0.904	-0.493 / 0.727
2 Node 825	-0.746	-0.099 / 0.116	-0.282 / 0.137	-0.420 / 0.438	-0.616 / 0.738
3 Node1041	-1.060	-0.184 / 0.217	-1.503 / 1.476	-0.452 / 0.803	-0.832 / 0.832

Inspection of Table 4 gives evidence that:

- the target first frequency is achieved;
- the companion torsional frequency is very close to the flexural ones;
- the four models come with significant differences in the upper frequencies.

Table 4 shows the axial force generated in the more stressed element (linked to the support) by the gravity load that must be added to the oscillating values recorded during the transient dynamic excitation. There is evidence of a correlation between the frequencies in Table 3 and the maximum oscillations in Table 4.

Moving to Fig. 7, restricted to the geodesic model, one has three lines in each of the four plots: the dotted line shows the horizontal displacement imposed at the soil level, different from zero along one half of the excitation duration; a thin (brown) line provides the horizontal displacement immediately atop the isolation device and a thick line gives the horizontal displacement at the dome top. The expected response for a base isolated system would come with an almost null response in the last two plots. It is seen that the base isolation behaves consistently for the input signals at 4 and 8 Hz. In the former case, however, the first dome couple sends the horizontal displacements in opposition to the phase at the top of the dome and the top of the isolation device, i.e., the relative displacement, which is an index of how the skeleton is stressed, is not negligible. The same

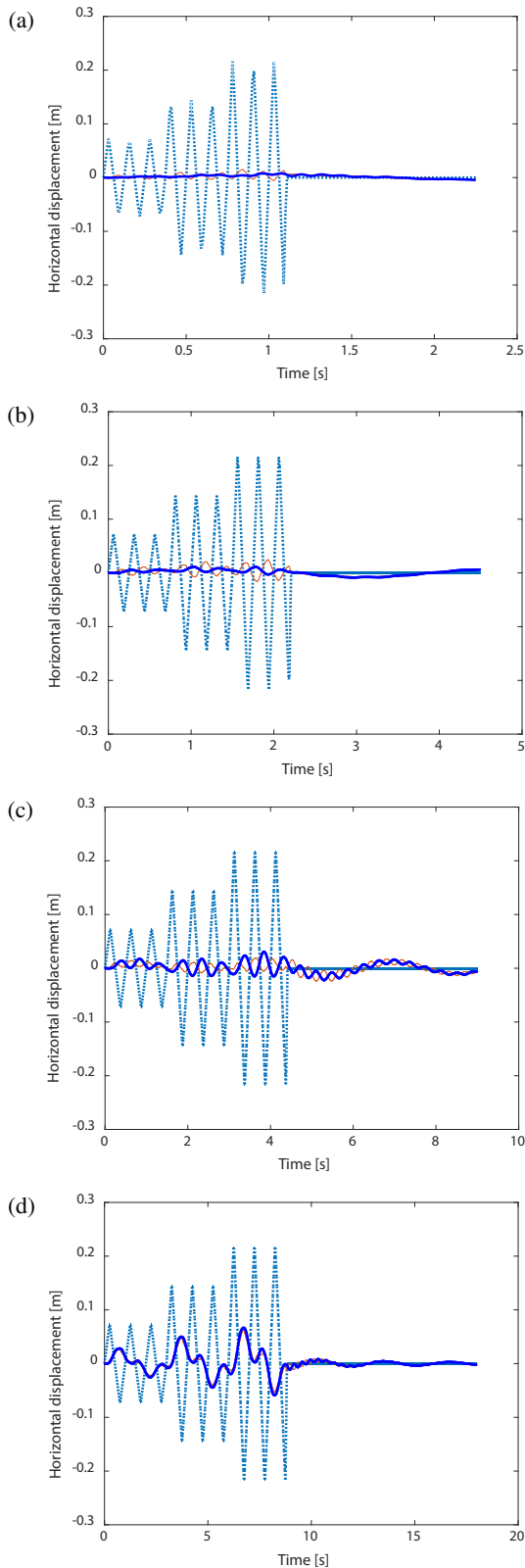


Fig. 7. Response time histories for the geodesic dome. The dotted line is the base excitation, the thin (brown) line denotes the movement at the top of the isolation device, and the thick line is the movement at the top of the dome: (a) 8 Hz; (b) 4 Hz; (c) 2 Hz and (d) 1 Hz. The base excitation, for the first half of its duration, consists of a series of three pulses, with intensity twice and three times the initial one, respectively, followed by a second half at rest

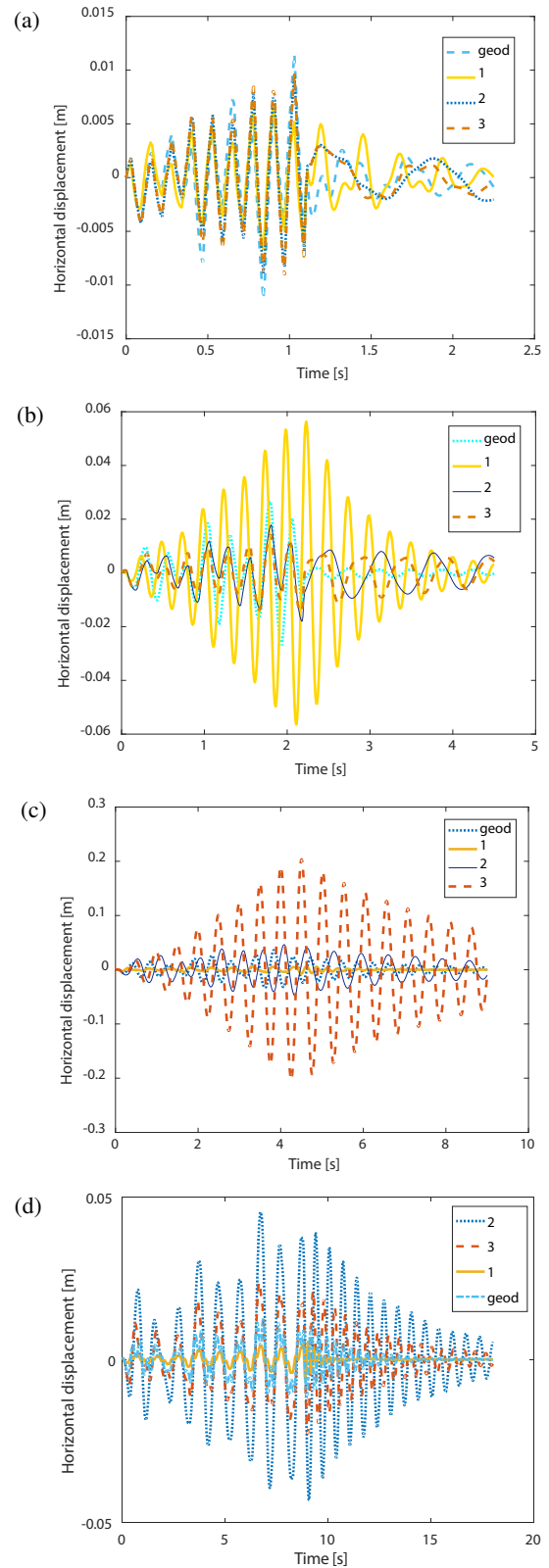


Fig. 8. Relative displacement time histories for the four proposed models. The plots provide the relative displacements between the top of the dome and the top of the isolation device: (a) 8 Hz; (b) 4 Hz; (c) 2 Hz and (d) 1 Hz. The line representing model 2 is solid and thin for cases b) and c). Graphical reasons suggested a dotted representation in the other two cases

behavior characterizes the situation with an input signal at 2 Hz, but in this case, the vibration of the dome is still alive also when the base is at rest. When inspecting the response to the signal at 1 Hz, one sees an even worse response in the absolute values, but the relative displacement is negligible.

One is ready now to start a comparison of the response for the four models. Figure 8 provides the relative displacements between the top of the dome and the top of the isolation device.

- When the input signal has a frequency of 8 Hz, Fig. 8a, the result is comparable for all the models and the base isolation quite effective.
- When the input signal has a frequency of 4 Hz, Fig. 8b, model 1 is not so effective. Table 4 shows in fact that the input sends in resonance a third couple of dome frequencies.
- When the input signal has a frequency of 2 Hz, Fig. 8c, it is model 3 that shows a bad performance. Again Table 4 gives the explication since the third dome couple is excited in this model. Figure 9 provides better evidence of how this misbehavior occurs.
- When the input signal has a frequency of 1 Hz, Fig. 8d, model 2 performs poorly. Again Table 4 gives an explanation since the first dome couple is excited in this model.

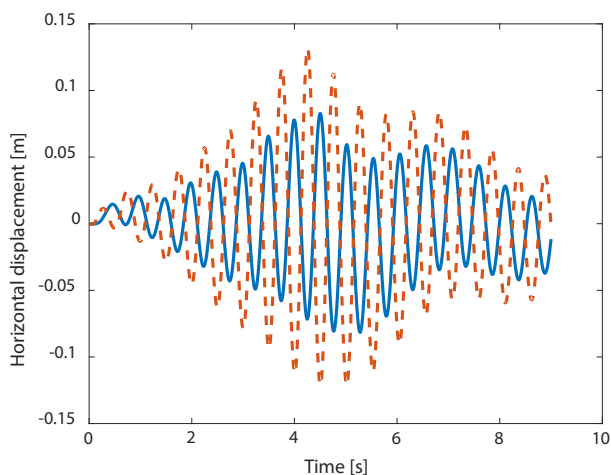


Fig. 9. Model 3. Response time histories to the signal of frequency 2 Hz. One sees the opposition of phase between the displacement at the top of the isolation device (dashed line) and the top of the dome (solid line)

Nevertheless, one cannot conclude that the geodesic model is the better one since it is likely to show misbehavior at different values of the frequency input.

The numerical simulations carried out in this paper emphasize that the difficulties to realize standard base isolation come from the economical impossibility of providing a quite stiff plate over the base isolation devices. This is a common problem for non-continuous homogeneous domes, also affecting continuous domes with ribs.

The design of base-isolated dome skeletons, therefore, requires either a careful scanning of the upper frequencies, required to be external to the excitation spectrum or the adoption of suitable dampers to smooth the resonance responses.

5. CONCLUSIONS

The paper analyzes the seismic performance of domes implemented as a transparent shield supported by a skeleton of steel tubular profiles. Different ways of drawing the skeleton are introduced with the constraints of:

- preserving the symmetry around two orthonormal axes and
- relying on eight supporting locations.

A base isolation solution is proposed. The inspiring technical realization was the new Apple Park in Texas: it has a circular plan and was base-isolated. In order to avoid the foundation plate, in this study the anchorage points are linked, each to the two neighbor ones, by a cable avoiding moving the devices out of phase. Such a solution is also compatible with the architectural access requirements that characterize the low part of the hemispherical dome.

Once it is stated that for each of the four proposed models the base isolation works adequately in terms of displacements, the models are compared among them in terms of the axial force oscillations in the bottom elements of the supporting skeleton.

The main conclusion is about the role of the upper frequencies that involve relative movements of the elements anchored to the supports. This is because the standard foundation plate coming with base-isolation devices is not economical in this case.

Future attention should be devoted to three main issues:

- the possibility of linking the anchorages with each other;
- the possibility of acting on the upper frequencies to move away from the excitation spectrum;
- the completion of the dome skeleton design by adding suitable dampers to smooth the negative effects of resonances under the upper frequencies.

REFERENCES

- [1] D. Losanno, C. Spizzuoco, and G. Serino, "Seismic isolation, monitoring, identification and modelling of the "Our Lady of Tears" shrine in Syracuse," *Progettazione Sismica*, vol. 5, no. 1, pp. 31–62, 2014, doi: [10.7414/PS.5.1.31-62](https://doi.org/10.7414/PS.5.1.31-62). (in Italian)
- [2] B. Basu, *et al.*, "A European Association for the Control of Structures joint perspective. Recent studies in civil structural control across Europe," *Struct. Control. Health Monit.*, vol. 21, no. 12, pp. 1414–1436, 2014.
- [3] S. Casciati and L. Faravelli, "An actively controlled prototype for educational buildings," *Smart. Struct. Syst.*, vol. 25, no. 1, pp. 105–109, 2020.
- [4] F. Casciati and S. Casciati, "Amelioration and retrofitting of educational buildings," *Earthq. Eng. Eng. Vib.*, vol. 17, no. 1, pp. 47–51, 2018.
- [5] S. Casciati, F. Casciati, and L. Faravelli, "Focus on the retrofit of educational buildings," *Proceedings ICONHIC (International Conference on Natural Hazards & Infrastructures) 2019*, Greece, 2019, p. 328.
- [6] A. Kaveh and S. Talatahari, "Geometry and topology optimization of geodesic domes using charged system search," *Struct. Multidiscip. Optim.*, vol. 43, no. 2, pp. 215–229, 2011.
- [7] S. Gholizadeh and H. Barati, "Topology optimization of nonlinear single layer domes by a new metaheuristic," *Steel Compos. Struct.*, vol. 16, no. 6, pp. 681–701, 2014.

- [8] A. Kaveh and M. Rezaei, "Topology and geometry optimization of different types of domes using ECBO," *Adv. Comput. Des.*, vol. 1, pp. 1–25, 2016, doi: [10.12989/acd.2016.1.1.001](https://doi.org/10.12989/acd.2016.1.1.001).
- [9] D. Pilarska, "Two subdivision methods based on the regular octahedron for single- and double-layer spherical geodesic domes," *Int. J. Space Struct.*, vol. 35, no. 4, pp. 160–173, 2020.
- [10] M.P. Saka, "Optimum geometry design of geodesic domes using harmony search algorithm," *Adv. Struct. Eng.*, vol. 10, no. 6, pp. 595606, 2007.
- [11] M. Babaei and M. R. Sheidai, "Automated optimal design of double-layer latticed domes using particle swarm optimization," *Struct. Multidiscip. Optim.*, vol. 50, pp. 221–235, 2014.
- [12] J. Ye and M. Lu, "Optimization of domes against instability," *Steel Compos. Struct.*, vol. 28, no. 4, pp. 427–438, 2018.
- [13] A. Kaveh, M. Rezaei, and M.R. Shiravand, "Optimal design of nonlinear large-scale suspendome using cascade optimization," *Int. J. Space Struct.*, vol. 33, no. 1, pp. 3–18, 2018.
- [14] Y. Guan, L.N. Virgin, and D. Helm, "Structural behavior of shallow geodesic lattice domes," *Int. J. Solids Struct.*, vol. 155, no. 15, pp. 225–239, 2018.
- [15] D. Pilarska and T. Maleska, "Numerical analysis of steel geodesic dome under seismic excitations," *Materials*, vol. 14, p. 4493, 2012, doi: [10.3390/ma14164493](https://doi.org/10.3390/ma14164493).
- [16] J. Li and J. Xu, "Dynamic stability and failure probability analysis of dome structures under stochastic seismic excitation," *Int. J. Struct. Stab. Dyn.*, vol. 14, no. 5, p. 1440001, 2014, doi: [10.1142/S021945541440001X](https://doi.org/10.1142/S021945541440001X).
- [17] J.K. Kelly, *Earthquake Resistant Design with Rubber*. Springer-Verlag, London, 1993.
- [18] F. Naeim and J.M. Kelly, *Design of Seismic Isolated Structures: From Theory to Practice*, John Wiley & Sons Inc., 1999.
- [19] L.A. Aghalovyan, A.V. Sahakyan, and M.L. Aghalovyan, "Analysis of layered bases-foundations models under seismic actions," *Smart. Struct. Syst.*, vol. 2, no. 4, pp. 295–304, 2006, doi: [10.12989/sss.2006.2.4.295](https://doi.org/10.12989/sss.2006.2.4.295).
- [20] A. Martelli and M. Forni, "Seismic isolation of civil buildings in Europe," *Prog. Struct. Eng. Mater.*, vol. 1, no. 3, pp. 286–294, 2005.
- [21] M.G. Melkumyan, "Seismic isolation experience accumulated in Armenia," in *Proc. of 14th World Conference on Earthquake Engineering*, China, 2008.
- [22] E. Alavi and M. Alidoost, "Soil-structure interaction effects on seismic behavior of base-isolated buildings," in *Proc. of 15th World Conference on Earthquake Engineering*, Portugal, 2012.
- [23] "Uniform Building Code, 1997," *International Conference of Building Officials*, Whittier, California, USA, 1997.